Author/s:
Ackland, DC;Robinson, DL;Wilkosz, A;Wu, W;Richardson, M;Lee, P;Tse, KM

Title:
The influence of rotator cuff tears on muscle and joint-contact loading after reverse total shoulder arthroplasty

Date:
2019-01-01

Citation:
Ackland, D. C., Robinson, D. L., Wilkosz, A., Wu, W., Richardson, M., Lee, P. & Tse, K. M. (2019). The influence of rotator cuff tears on muscle and joint-contact loading after reverse total shoulder arthroplasty. Journal of Orthopaedic Research, 37 (1), pp.211-219. https://doi.org/10.1002/jor.24152.

Persistent Link:
https://hdl.handle.net/11343/284554

Research Article (Member)

The influence of rotator cuff tears on muscle and joint-contact loading after reverse total shoulder arthroplasty[1]

[1]David Charles Ackland, [1]Dale Lee Robinson, [1]Adam Wilkosz, [1]Wen Wu,

[2]Martin Richardson, [1]Peter Lee, [1]Kwong Ming Tse 0000-0002-8170-0775 0000-0002-8170-0775

[1]Department of Biomedical Engineering, University of Melbourne, Victoria, Australia
[2]Epworth Healthcare, Richmond, Victoria, Australia

Submitted as an **Original Article** to *Journal of Orthopaedic Research*

Address for correspondence:

David C. Ackland

Department of Biomedical Engineering

University of Melbourne

Parkville, Victoria, 3010, Australia

Phone: +613 8344 8646

Fax: +613 9347 8784

Email: dackland@unimelb.edu.au

[1] This is the author manuscript accepted for publication and has undergone full peer review but has not been through the copyediting, typesetting, pagination and proofreading process, which may lead to differences between this version and the Version of Record. Please cite this article as doi:10.1002/jor.24152

Running title: Joint loading after reverse shoulder arthroplasty

Keywords: glenohumeral joint; deltoid; joint torque; upper limb; prosthesis; finite element; biomechanical model

Abstract
Rotator cuff tears are known to affect clinical outcome of reverse total shoulder arthroplasty (RSA). This study aimed to use computational modelling to quantify the effect of rotator cuff tear severity on muscle and joint forces after RSA, as well as stresses at the glenosphere, base-plate, fixation screws, scapula, and humeral components. A multi-body musculoskeletal model of the glenohumeral joint was developed comprising the scapula, humerus and 9 major upper limb muscles. Simulations of abduction and flexion were performed after RSA with the intact rotator cuff and tears to (i) supraspinatus (ii) supraspinatus and infraspinatus (iii) supraspinatus, infraspinatus and subscapularis. The intact and supraspinatus deficient rotator cuff resulted in the largest calculated muscle forces, glenohumeral joint contact forces and implant stresses. Peak glenohumeral joint forces during flexion were lower than those during abduction in all cases; however, substantially more posterior joint shear force was generated during flexion than abduction. A combined supraspinatus and infraspinatus tear reduced glenohumeral joint forces by a factor of 8.7 during abduction (603.1 N) and 7.1 during flexion (520.7 N) compared to the supraspinatus deficient shoulder. RSA with an intact or supraspinatus deficient rotator cuff produces large glenohumeral joint forces that may increase base-plate failure risk, particularly during flexion when posterior shear forces are largest. Infraspinatus tears after RSA greatly reduce glenohumeral joint compression and may ultimately reduce joint stability. Given the inherent uncertainty of musculoskeletal model calculations, future research ought to focus on experimental validation of subject-specific muscle recruitment strategies and joint loading after RSA.

INTRODUCTION

Reverse total shoulder arthroplasty (RSA) has traditionally been a salvage procedure for patients with end-stage rotator cuff tear arthropathy[1], but is now widely used in cases of pseudoparalysis with massive irreparable rotator cuff tears [2,3], tumour resection[4,5], trauma where the proximal humerus is destroyed or absent[6,7], and revision arthroplasty in a rotator cuff deficient shoulder[8,9]. The reverse shoulder prosthesis has been shown to relocate the glenohumeral joint center of rotation medially and inferiorly by 20.9 mm and 10.3 mm, respectively[10]. This has the effect of tensioning the deltoid, recruiting more of its fibres and increasing its moment arms during elevation motions such as abduction and flexion[11]. While RSA may reduce pain, improve upper limb strength and increase range of shoulder motion, complication rates have ranged between 10% and 68%[12], with substantially higher prevalence associated with revision surgery[3,13].

Glenohumeral joint force is a function of the resultant load generated by each muscle spanning the joint, and is an important predictor of joint stability by concavity compression of the articulating joint surfaces. In the native shoulder, the superior glenohumeral joint force generated by the deltoid during early- to mid-elevation is balanced by the inferior-directed forces of the rotator cuff muscles resulting in a stabilizing scapular-plane force couple, while the anterior and posterior rotator cuff muscles simultaneously activate to generate a stabilizing transverse-plane force-couple[14]. In the reverse shoulder, irreparable tears to the rotator cuff tendons can result in greater risk of joint subluxation or early loosening of the glenoid-side component[1,15-17]. This may arise from disruption in the stabilizing capacity of the normal functioning rotator cuff and reduced glenohumeral joint compression. While it has been shown that rotator cuff repair in conjunction with joint lateralization may ultimately increase deltoid and glenohumeral

joint loading[18], the relationship between rotator cuff tears and the compressive and shear forces generated at the glenohumeral joint after RSA is not well understood.

Computational modelling is an established and widely employed technique for quantifying muscle and joint loading in the upper limb. Three-dimensional rigid-body musculoskeletal models have been used to investigate biomechanics of the shoulder after RSA, including muscle length and moment arm properties[19,20], glenohumeral joint contact forces and impingement[21], and muscle and joint forces during activities of daily living[22], while finite element modelling has been employed to investigate the influence of global rotator cuff tears on muscle and joint force during abduction[23]. Musculoskeletal modelling has also demonstrated a decrease in the peak compressive and shear components of the glenohumeral joint force after RSA[21], and an increase in the superior component of the glenohumeral joint force in the presence of a global rotator cuff tear[23], findings also observed in a cadaveric model of a posterosuperior rotator cuff tear[24]. Loss of active rotator cuff depressor function increases the potential of the glenohumeral joint to sublux superiorly under the action of the deltoid; however, the resulting load transmitted to the base-plate, fixation screws and bone has not been investigated to date. Eccentric glenohumeral joint loads generated as a consequence of rotator cuff tearing may ultimately present a risk factor for joint instability and periprosthetic fracture, which are the most common complications of RSA[25].

The aim of this study was to develop and validate a computational model of the shoulder to assess the influence of progressive rotator cuff tears on muscle and joint-contact loading during abduction and flexion after RSA, including the stresses produced at the glenosphere, base-plate, fixation screws, scapula, and humeral components. A

multi-body computational model was developed, comprising a rigid-body musculoskeletal model for estimating neuromuscular function, and a finite element model for calculating resultant joint-contact forces and implant stresses. The results may indicate rotator cuff tears that place the reverse shoulder at greatest risk of implant loosening, joint instability, and dislocation, which are among the most commonly observed complications of RSA[25].

METHODS

Rigid-body musculoskeletal model

A previously published 5-segment, 10-degree-of-freedom (DOF) rigid-body musculoskeletal model of a 92 kg male upper limb was developed in OpenSim and based on the Visible Human Male (VHM) anatomy (Figure 1A)[26-29]. The glenohumeral and acromioclavicular joints were modelled as 3-DOF ball and socket joints, the sternoclavicular joint as a 2-DOF universal joint, and the elbow joint as a 2-DOF universal joint. The shoulder complex was actuated by 26 Hill-type muscle-tendon units representing the axioscapular (levator scapulae, superior trapezius, lower-middle trapezius, lower trapezius, rhomboid minor, superior rhomboid major, lower rhomboid major, superior serratus anterior, middle serratus anterior, lower serratus anterior, subclavius, pectoralis minor), axiohumeral (teres major, superior pectoralis major, middle pectoralis major, lower pectoralis major, latissimus dorsi) and scapulohumeral muscles (anterior deltoid, middle deltoid, posterior deltoid, supraspinatus, infraspinatus, subscapularis, teres minor, coracobrachialis). The timing of the prime mover muscle activations in the native shoulder showed high agreement with muscle EMG onset and

offset data obtained from healthy individuals[29], while glenohumeral joint force magnitude calculations have been shown to match closely those calculated using previous instrumented shoulder implant data[30].

To simulate the anatomy of the shoulder after RSA, the glenohumeral joint centre was displaced medially and inferiorly by 20.9 mm and 10.3 mm, respectively[10]. An optimization procedure was then developed to determine optimal muscle paths and wrapping 'via point' locations in order to match the model's muscle moment arms and lines of action with those measured on 8 cadaveric upper extremities after RSA[10,24,31]. Specifically, a numerical optimiser minimised the sum of squared differences between the simulated moment arms and anatomically measured muscle moment arms through the entire range of humeral abduction, flexion and internal-external rotation. The initial guesses of the 'via-point' locations were determined by setting the anatomical muscle path to that of the VHM. The 'via-point' locations were constrained within 1.5 cm of the initial guess and were also adjusted to ensure replication of each muscle-tendon unit's lines of action. Musculotendon parameters, including optimum muscle fiber lengths and tendon slack lengths, were scaled in equal proportion from previously calculated values to ensure a match in muscle-tendon unit length with the VHM[32], while maximum isometric muscle force values were scaled in proportion to maximum muscle cross-sectional area. Segment mass, center of mass location and inertial properties were calculated using previously published anatomical data[32].

The average upper limb kinematics measured in six healthy male subjects (age: 25–38 yrs, height: 170–175 cm, mass: 56–85 kg)[28] was then employed in nominal model simulations of scapular-plane abduction and sagittal-plane flexion to calculate shoulder

muscle forces and glenohumeral joint contact forces. Muscle forces were computed using static optimisation in Matlab 2014 (Mathworks, US) by minimizing the sum of the squares of muscle activations subject to constraints on each muscle's force-length and force-velocity relations. A variable anisotropic elliptical shape ratio was employed to constrain the calculated glenohumeral joint force direction and simulate rotator cuff muscle co-contraction. Specifically, compressive (F_c), anterior (F_a) and superior components of the GH joint force (F_s) were computed and constrained using

$$\frac{F_s^2}{a^2} + \frac{F_a^2}{b^2} \leq F_c^2$$

where the constants a=0.61 and b=0.34 were obtained from Lippitt and Matsen (1993)[33]. The model was subsequently used to estimate muscle forces with the intact rotator cuff and for the following rotator cuff conditions: (i) isolated tear to the supraspinatus (ii) tear to the supraspinatus and infraspinatus (iii) tear to the supraspinatus, infraspinatus and subscapularis, and (iv) global tear involving all rotator cuff tendons.

Finite element model

A three-dimensional finite element model of the upper limb implanted with the Trabecular Metal Reverse Shoulder System (Zimmer-Biomet, Warsaw, United States) was developed using commercially available software (Abaqus, Dassault Systems, France). The scapula and humerus geometry were obtained by digitally segmenting and reconstructing axial images of the VHM upper limb (Amira, FEI, France). The bony anatomy and prosthetic components were meshed using tetrahedral elements (Hypermesh, Altair, United States) with linear-elastic material properties based on previously reported values (see Supplementary Material). Scapula motion and humeral elevation angle were prescribed according to the measured kinematics, while the

glenohumeral joint was free to move in the remaining five degrees of freedom. Each muscle's force calculated throughout abduction and flexion was applied across the area of distal attachment of the muscle in the direction of its line of action.

Simulations

RSA using the Trabecular Metal Reverse Shoulder System was performed virtually using the finite element model (Figure 1B), and post-operative joint-contact and implant loading evaluated. Arthroplasty was performed according to the recommended Zimmer technique. Briefly, a humeral head resection was performed at a 53° angle relative to the long-axis of the humerus, and the proximal humeral canal prepared (reamed) to match a 16 mm humeral implant of length 170 mm with 0° retroversion. A 36 mm ultra-high molecular weight polyethylene (UHMWPE) liner with 3mm offset was rigidly fixed to the proximal humeral stem. There was no prosthetic overhang at the proximal humerus. The glenoid was reamed as inferiorly as possible to accommodate the 15mm base-plate and its central peg without interference of the glenosphere with the supraglenoid tubercle. Two 40 mm length oblique fixation screws were inserted in the base-plate at a 20° angle in the coronal plane with the superior screw placed just below the supraglenoid tubercle and the inferior screw just above the infraglenoid tubercle. A 36 mm glenosphere was rigidly attached to the base plate without inferior glenoid overhang, and the glenohumeral joint centre of rotation medialized by 21 mm, as reported previously[24]. The resultant humeral lateralization calculated at 15° of abduction was 15.2 mm.

The metal-screw and metal-bone interfacial conditions were assumed to be sliding contact, with coefficients of friction defined as 0.1 for screw-to-base-plate contact, 0.42

for screw-to-scapula contact, and 0.98 for base-plate-to-scapula contact[34,35]. Post-operative muscle forces calculated using the rigid-body musculoskeletal model were applied to the finite element model during quasi-static simulations of abduction and flexion performed at 0°, 45° and 90° of abduction and flexion. Simulations were performed in the case of the intact rotator cuff, and for the four rotator cuff tear cases. Glenohumeral joint contact force, as well as von Mises stress at the glenosphere, base-plate, fixation screws, humeral stem and humeral liner, were subsequently calculated. To quantify the amount of shear to compressive force at the glenohumeral joint after RSA, Anterior Joint Force Ratios (AJFR) and Superior Joint Force Ratios (SJFR) were computed, defined by the percentage of anterior and superior glenohumeral joint force to compressive joint force, respectively.

To validate the muscle and joint architecture employed in the finite element model, simulated abduction and flexion experiments were performed on 8 fresh-frozen entire upper extremities implanted with the Trabecular Metal Reverse Shoulder System (Zimmer-Biomet, Warsaw, United States). The resultant glenohumeral joint forces were then compared with those calculated from simulations performed with the finite element model using the same system of muscle forces and joint positions (see Supplementary Material).

RESULTS

Intact rotator cuff

With the rotator cuff intact, the middle deltoid was the greatest producer of muscle force after RSA, demonstrating a force peak of 240.7 N and 182.4 N at 90° of abduction and flexion, respectively (Table 1). The infraspinatus also generated substantial

force, particularly at 90° of abduction and flexion (214.2 N and 242.6 N, respectively). During abduction, the glenohumeral joint contact force magnitude peaked at 45° (612.5 N), but little superior-inferior joint force was generated (maximum SJFR: 10.8% at 45°) nor anterior-posterior joint contact force (maximum AJFR: -4.8% at 90°) (Table 2). In contrast, the glenohumeral joint force magnitude peak during flexion was lower (490.5 N at 45°), although substantial posterior shear force was generated (maximum AJFR: -110.7% at 90°) (Table 3). The superior fixation screw experienced greater stress than the inferior screw during abduction and flexion, for example, 159.3 MPa (superior screw) vs 12.1 MPa (inferior screw) at 90° of abduction. Base plate stresses were highest at 90° of abduction (21.1 MPa) and 90° of flexion (18.1 MPa).

Supraspinatus tear

An isolated supraspinatus tear after RSA resulted in larger muscle forces, glenohumeral joint forces, base plate stresses, screw stresses, and scapular stresses than with the intact rotator cuff or any other rotator cuff tear case. Tearing to the supraspinatus resulted in force increases in the middle deltoid (41.8 N), infraspinatus (83.0 N) and subscapularis (82.5 N) at 15° of abduction, and force increases in the middle deltoid (51.9 N), infraspinatus (70.4 N) and subscapularis (90.4 N) at 15° of flexion relative to the intact rotator cuff condition (Table 1). Peak glenohumeral joint force magnitude was larger in the case of the isolated supraspinatus tear than in the intact rotator cuff during abduction (difference: 98.1 N) and flexion (difference: 115.8 N) (Tables 2 and 3). There were negligible changes in AJFR and SJFR in the case of a supraspinatus tear. However, superior fixation screw stresses increased by up to 14.7 MPa during abduction and 21.2 MPa during flexion. Relative to the intact rotator cuff, the peak stresses in the

glenosphere, base plate, humeral spacer and humeral stem increased by just small amounts in the presence of an isolated supraspinatus tear (<8 MPa).

Supraspinatus and infraspinatus tear

A rotator cuff tear involving both the supraspinatus and infraspinatus after RSA resulted in higher forces generated by the anterior deltoid, but vastly reduced glenohumeral joint force magnitudes, and markedly lower base plate and fixation screw stresses relative to those with the intact rotator cuff or in the presence of an isolated supraspinatus tear. The maximum force in the anterior deltoid during abduction and flexion was 124.2 N and 144.4 N larger than that in the supraspinatus deficient shoulder, respectively (Table 1). The glenohumeral joint force magnitude in the case of a combined supraspinatus and infraspinatus tear during abduction was up to 8.7 times smaller (603.1 N) than that in the supraspinatus deficient shoulder (Table 2). During flexion, the glenohumeral joint force magnitude dropped by a factor of 7.1 (520.7 N) relative to that in the supraspinatus deficient shoulder (Table 3). AJFR was not substantially different during abduction and flexion; however, SJFR was superiorly directed in the case of a tear to the supraspinatus and infraspinatus, but inferiorly directed in the case of a supraspinatus tear. The peak stresses in the superior fixation screw during abduction (flexion) reduced from 159.0 MPa (147.7 MPa) in the supraspinatus deficient shoulder to 113.1 MPa (66.0 MPa) in the case of the combined supraspinatus and infraspinatus tear. Relative to the supraspinatus deficient shoulder, the peak stresses at the glenosphere, base plate, humeral spacer and humeral stem during abduction were up to 20.8 MPa, 10.2 MPa, 7.2 MPa and 9.1 MPa lower in the presence of a combined supraspinatus and infraspinatus tear, respectively. During flexion, glenosphere, base plate, humeral spacer

and humeral stem stresses were lower by 19.4 MPa, 8.4 MPa, 6.1 MPa, and 2.5 MPa, respectively.

Supraspinatus, infraspinatus and subscapularis tear

Increasing the supraspinatus and infraspinatus tear anteriorly to involve the subscapularis did not substantially alter the deltoid forces, the glenohumeral joint forces and AJFR and SJFR during abduction and flexion. There was also little change to the stresses in the screws, base plate, humeral spacer and humeral stem. While there was some reduction in the glenohumeral joint force magnitude at 90° of flexion (difference: 26.8 N), there were no discernable changes in implant stresses observed during abduction or flexion when increasing a combined supraspinatus and infraspinatus tear to also involve the subscapularis.

Supraspinatus, infraspinatus, subscapularis and teres minor tear

A global tear to the rotator cuff demonstrated no change in muscle forces relative to those in the cases of the supraspinatus-infraspinatus-subscapularis tear during abduction and flexion; however, glenohumeral joint force magnitudes were up to 83.3 and 22.8 N lower during abduction and flexion, respectively. AJFR, SJFR and implant stresses were not affected.

DISCUSSION

One of the most common indications for RSA is rotator cuff tear arthropathy involving irreparable tendon tears as a consequence of poor tissue substrate for repair or muscle fatty infiltration[36]. Loss of rotator cuff function in the reverse shoulder may ultimately compromise glenohumeral joint compression and increase risk of

glenohumeral joint dislocation, while an intact rotator cuff may excessively load the base-plate and contribute to screw breakage, pull-out or baseplate migration[1,37]. While shoulder muscle and joint-contact forces after RSA have been estimated using experimental approaches and computational modelling[21,23,24,38,39], and the influence of rotator cuff repair on muscle and glenohumeral joint loading quantified in a cadaver model[18], the influence of rotator cuff tears on implant load response is not well understood. The objective of this study was therefore to quantify the influence of progressively severe rotator cuff tears on muscle and joint loading, and implant stresses at the base-plate and fixation screws after RSA.

The present study showed that RSA with an intact or supraspinatus deficient rotator cuff leads to high glenohumeral joint forces post-operatively due to the combined activity of the rotator cuff and the deltoid when the upper limb is elevated under its own weight. Peak glenohumeral joint forces in the case of the intact rotator cuff (612.5 N and 490.5 N during abduction and flexion, respectively) were shown to increase in the presence of an isolated supraspinatus tear (increase: 98.1 N and 115.8 N during abduction and flexion, respectively). Greater middle deltoid force was required to compensate for the torn supraspinatus, particularly during early abduction and flexion, with additional activation of the infraspinatus and subscapularis to offset the greater superior shear generated by the deltoid. In this manner, RSA in the presence of a torn supraspinatus produces larger glenohumeral joint forces resulting in higher stresses at the glenosphere, base plate, and fixation screws than any other rotator cuff tear configuration. The findings suggest that both an intact and supraspinatus deficient rotator cuff represent a ‘balanced’ glenohumeral joint[40] which, under the large combined joint load generated by the anterior

(subscapularis) and posterior rotator cuff muscles (infraspinatus, teres minor), and the semi-constrained nature of the glenohumeral joint articulation, may present a risk factor for early loosening or failure of the glenoid-side component.

The present study showed that relatively little superior-inferior or anterior-posterior glenohumeral joint shear force was generated during abduction with the intact rotator cuff, or in the presence of any tears involving the supraspinatus, infraspinatus, subscapularis or teres minor. While tears to these tendons during abduction resulted in superior joint shear forces under the action of the deltoid at low abduction angles where its superior inclination is maximal (e.g., 11.4 N at 15º of abduction in the case of a torn supraspinatus and infraspinatus), the superior shear force generated was relatively small. Deltoid force generation is minimal at initiation of abduction, and peaks at 90º of abduction whereupon its line of action favors joint compression and not shear.

During flexion, the humerus is positioned in the sagittal plane with the line of action of the deltoid sub-regions directed posteriorly toward the clavicle, acromion and scapular spine. As the deltoid is increasingly activated during elevation in the sagittal plane, substantial posterior glenohumeral joint shear is generated, especially at 90º of flexion when anterior deltoid force is maximal (Tables 1 and 3). More posterior glenohumeral joint shear was generated during flexion than abduction, particularly when the infraspinatus was torn and the transverse-plane force-couple disrupted. These findings suggest that elevation of the shoulder in the sagittal plane after RSA may present greater risk of instability and dislocation than elevation in the scapular plane. Post-operatively rehabilitation exercises ought to focus on elevation tasks in the scapular plane at low

elevation angles to develop strength in the anterior and middle deltoid, while reducing joint shear forces and the risk of early base-plate loosening.

Both an intact and supraspinatus deficient rotator cuff resulted in large calculated joint forces at the glenosphere after RSA; however, extension of a supraspinatus tear to involve the infraspinatus produced glenohumeral joint force magnitudes that were a factor of 8.7 and 7.1 smaller than those in the supraspinatus deficient shoulder during abduction and flexion, respectively. This significant drop in joint loading was not substantially affected by further tearing to the subscapularis and teres minor, and resulted in substantially smaller base plate and fixation screw stresses, as well as smaller humeral component stresses relative to those in the intact or supraspinatus deficient rotator cuff. Loss of function of the infraspinatus resulted in a muscle recruitment pattern that preferentially deactivated the subscapularis in order to maintain a muscle torque-balance in the transverse plane, thus contributing to the lower glenohumeral joint loads. While the consequence of small glenohumeral joint forces after RSA may be reduced likelihood of early loosening and failure of the base-plate, reduced joint compression may ultimately increase joint instability, which is common and debilitating complication of RSA[41]. Specifically, loss of compressive glenohumeral joint force may leave the glenohumeral joint prone to subluxation, particularly after intra-operative over-tension of the deltoid[42,43], or in cases of impact loads sustained in the upper limb.

Glenohumeral joint force calculations using the finite element model were compared to those measured from joint motion experiments performed on entire-upper extremities that had undergone RSA. Model predictions of glenohumeral joint forces during abduction and flexion showed high levels of agreement with experimentally

measured values at low elevation, and increased divergence at larger angles when greater muscle forces were required. These discrepancies may be a consequence of the different muscle architecture and joint anatomy between the musculoskeletal model and the cadaveric upper extremities, differing strategies employed in estimating joint force between experiments and model simulations, and possible variations in surgical placement of the prostheses in cadaveric specimens.

There are a number of limitations of this study that ought to be considered when interpreting the findings. First, clinically relevant progressive tears to the rotator cuff were investigated, from the intact rotator cuff to a global rotator cuff tear; however, there may be other isolated or combined rotator cuff tears and reconstructions not considered, producing different patterns of glenohumeral joint force and implant loading[15]. This includes tendon transfers to restore humeral rotation function, including latissimus dorsi and teres major tendon transfer for external rotation deficit[44] and pectoralis major tendon transfer for internal rotation deficit[45]. Second, when calculating muscle forces after RSA, static optimization was performed using a variable constraint on the glenohumeral joint force direction, which assumed a muscle recruitment strategy that has been validated in the native shoulder using EMG[29]. Further research is required to evaluate patterns of muscle activity after RSA and motor control strategies that occur in the presence of rotator cuff tears. Third, the conjoined tendon of the coracobrachialis and short-head of biceps was not explicitly modelled, and may ultimately contribute to glenohumeral joint stability[46]; however, further investigation into active and passive force-producing properties of its associated musculature in the reverse shoulder is required. Finally, the scapula and humerus were modelled with homogeneous isotropic material properties [47,48],

and this may underestimate localized bone stresses at the implant-screw interface; however, this is unlikely to influence the relative load patterns between the screws. We showed that the superior base-plate fixation screw experienced substantially larger stresses than those in the inferior screw, which may be explained by the glenosphere contact force bending the baseplate inferiorly and increasing the tensile and bending loads at the superior screw.

In conclusion, RSA in the presence of an intact rotator cuff or an isolated supraspinatus tear results in large glenohumeral joint forces, base plate stresses, screw stresses, and scapular stresses, and may ultimately present greater risk of glenoid-side component failure, particularly during flexion when posterior shear forces are largest. A tear to the supraspinatus and infraspinatus disrupts the transverse-plane rotator cuff force couple, resulting in a substantially smaller glenohumeral joint force magnitudes than in the case of an intact rotator cuff or isolated supraspinatus tear. This may ultimately present increased likelihood of joint instability or subluxation in cases of overtensioning of the deltoid, or when high external loads are applied to the upper limb. The findings may help to guide intra-operative component placement and rehabilitation to minimise the risk of early implant loosening, component failure or joint dislocation. While the data reported in the present study are based on established computational modelling and simulation techniques frequently employed in the anatomic shoulder, there is significant uncertainty in the predicted muscle loads, since it is currently not possible to measure and validate muscle forces non-invasively. Future studies ought to focus on evaluating subject-specific muscle recruitment strategies and quantifying joint force predictions in the reverse shoulder.

References

1. Wall B, Nove-Josserand L, O'Connor DP, et al. 2007. Reverse total shoulder arthroplasty: a review of results according to etiology. J Bone Joint Surg Am 89:1476-1485.
2. Neri BR, Chan KW, Kwon YW. 2009. Management of massive and irreparable rotator cuff tears. J Shoulder Elbow Surg 18:808-818.
3. Werner CM, Steinmann PA, Gilbart M, et al. 2005. Treatment of painful pseudoparesis due to irreparable rotator cuff dysfunction with the Delta III reverse-ball-and-socket total shoulder prosthesis. J Bone Joint Surg Am 87:1476-1486.
4. De Wilde L, Boileau P, Van der Bracht H. 2011. Does reverse shoulder arthroplasty for tumors of the proximal humerus reduce impairment? Clin Orthop Relat Res 469:2489-2495.
5. De Wilde LF, Plasschaert FS, Audenaert EA, et al. 2005. Functional recovery after a reverse prosthesis for reconstruction of the proximal humerus in tumor surgery. Clin Orthop Relat Res:156-162.
6. Bufquin T, Hersan A, Hubert L, et al. 2007. Reverse shoulder arthroplasty for the treatment of three- and four-part fractures of the proximal humerus in the elderly: a prospective review of 43 cases with a short-term follow-up. J Bone Joint Surg Br 89:516-520.
7. Klein M, Juschka M, Hinkenjann B, et al. 2008. Treatment of comminuted fractures of the proximal humerus in elderly patients with the Delta III reverse shoulder prosthesis. J Orthop Trauma 22:698-704.

8. Levy JC, Virani N, Pupello D, et al. 2007. Use of the reverse shoulder prosthesis for the treatment of failed hemiarthroplasty in patients with glenohumeral arthritis and rotator cuff deficiency. J Bone Joint Surg Br 89:189-195.

9. Boileau P, Watkinson D, Hatzidakis AM, et al. 2006. Neer Award 2005: The Grammont reverse shoulder prosthesis: results in cuff tear arthritis, fracture sequelae, and revision arthroplasty. J Shoulder Elbow Surg 15:527-540.

10. Ackland DC, Roshan-Zamir S, Richardson M, et al. 2010. Moment arms of the shoulder musculature after reverse total shoulder arthroplasty. J Bone Joint Surg Am 92:1221-1230.

11. Ackland DC, Patel M, Knox D. 2015. Prosthesis design and placement in reverse total shoulder arthroplasty. Journal of orthopaedic surgery and research 10:101.

12. Wierks C, Skolasky RL, Ji JH, et al. 2009. Reverse total shoulder replacement: intraoperative and early postoperative complications. Clin Orthop Relat Res 467:225-234.

13. Matsen FA, 3rd, Boileau P, Walch G, et al. 2007. The reverse total shoulder arthroplasty. J Bone Joint Surg Am 89:660-667.

14. Ackland DC, Pandy MG. 2009. Lines of action and stabilizing potential of the shoulder musculature. J Anat 215:184-197.

15. Edwards TB, Williams MD, Labriola JE, et al. 2009. Subscapularis insufficiency and the risk of shoulder dislocation after reverse shoulder arthroplasty. J Shoulder Elbow Surg 18:892-896.

16. Boileau P, Watkinson DJ, Hatzidakis AM, et al. 2005. Grammont reverse prosthesis: design, rationale, and biomechanics. J Shoulder Elbow Surg 14:147S-161S.

17. Lam F, Bhatia DN, Mostofi SB, et al. 2007. Biomechanical considerations of the normal and rotator cuff deficient shoulders and the reverse shoulder prosthesis. Current Orthopaedics 21:40-46.

18. Giles 0000-0001-6997-8873 0000-0001-6997-8873 JW, Langohr GD, Johnson JA, et al. 2016. The rotator cuff muscles are antagonists after reverse total shoulder arthroplasty. J Shoulder Elbow Surg 25:1592-1600.

19. Hamilton MA, Roche CP, Diep P, et al. 2013. Effect of prosthesis design on muscle length and moment arms in reverse total shoulder arthroplasty. Bull Hosp Jt Dis (2013) 71 Suppl 2:S31-35.

20. Roche CP, Diep P, Hamilton M, et al. 2013. Impact of inferior glenoid tilt, humeral retroversion, bone grafting, and design parameters on muscle length and deltoid wrapping in reverse shoulder arthroplasty. Bull Hosp Jt Dis (2013) 71:284-293.

21. Kontaxis A, Johnson GR. 2009. The biomechanics of reverse anatomy shoulder replacement--a modelling study. Clin Biomech (Bristol, Avon) 24:254-260.

22. Masjedi M, Johnson GR. 2010. Glenohumeral contact forces in reversed anatomy shoulder replacement. J Biomech 43:2493-2500.

23. Terrier A, Reist A, Merlini F, et al. 2008. Simulated joint and muscle forces in reversed and anatomic shoulder prostheses. J Bone Joint Surg Br 90:751-756.

24. Ackland DC, Roshan-Zamir S, Richardson M, et al. 2011. Muscle and joint-contact loading at the glenohumeral joint after reverse total shoulder arthroplasty. J Orthop Res 29:1850-1858.

25. Bohsali KI, Bois AJ, Wirth MA. 2017. Complications of Shoulder Arthroplasty. J Bone Joint Surg Am 99:256-269.

26. Spitzer V, Ackerman MJ, Scherzinger AL, et al. 1996. The visible human male: a technical report. J Am Med Inform Assoc 3:118-130.

27. Wu W, Fong J, Chrocher V, et al. 2018. Modulation of shoulder muscle and joint function using a powered upper-limb exoskeleton. J Biomech (Accepted 31st Jan, 2018).

28. Wu W, Lee PV, Ackland DC. 2017. The sensitivity of shoulder muscle and joint force predictions to changes in joint kinematics: A Monte-Carlo analysis. Gait Posture 54:87-92.

29. Wu W, Lee PV, Bryant A, et al. 2016. Subject-specific musculoskeletal modeling in the evaluation of shoulder muscle and joint function. J Biomech 49:3623-3634.

30. Bergmann G, Graichen F, Bender A, et al. 2007. In vivo glenohumeral contact forces--measurements in the first patient 7 months postoperatively. J Biomech 40:2139-2149.

31. Ackland DC, Richardson M, Pandy MG. 2012. Axial rotation moment arms of the shoulder musculature after reverse total shoulder arthroplasty. J Bone Joint Surg Am 94:1886-1895.

32. S. P, Evans FG, T. A. 1983. Anatomical Data for Analyzing Human Motion. Research Quarterly Exercise Sport 54:169-178.

33. Lippitt S, Matsen F. 1993. Mechanisms of glenohumeral joint stability. Clin Orthop Relat Res 291:20-28.

34. Viceconti M, Muccini R, Bernakiewicz M, et al. 2000. Large-sliding contact elements accurately predict levels of bone-implant micromotion relevant to osseointegration. J Biomech 33:1611-1618.

35. Shirazi-Adl A, Dammak M, Paiement G. 1993. Experimental determination of friction characteristics at the trabecular bone/porous-coated metal interface in cementless implants. J Biomed Mater Res 27:167-175.

36. Frankle M, Siegal S, Pupello D, et al. 2005. The Reverse Shoulder Prosthesis for glenohumeral arthritis associated with severe rotator cuff deficiency. A minimum two-year follow-up study of sixty patients. J Bone Joint Surg Am 87:1697-1705.

37. Holcomb JO, Cuff D, Petersen SA, et al. 2009. Revision reverse shoulder arthroplasty for glenoid baseplate failure after primary reverse shoulder arthroplasty. J Shoulder Elbow Surg 18:717-723.

38. Gutierrez S, Walker M, Willis M, et al. 2011. Effects of tilt and glenosphere eccentricity on baseplate/bone interface forces in a computational model, validated by a mechanical model, of reverse shoulder arthroplasty. J Shoulder Elbow Surg 20:732-739.

39. Henninger HB, Barg A, Anderson AE, et al. 2012. Effect of lateral offset center of rotation in reverse total shoulder arthroplasty: a biomechanical study. J Shoulder Elbow Surg 21:1128-1135.

40. Drake GN, O'Connor DP, Edwards TB. 2010. Indications for reverse total shoulder arthroplasty in rotator cuff disease. Clin Orthop Relat Res 468:1526-1533.

41. Zumstein MA, Pinedo M, Old J, et al. 2011. Problems, complications, reoperations, and revisions in reverse total shoulder arthroplasty: a systematic review. J Shoulder Elbow Surg 20:146-157.

42. Walch G, Mottier F, Wall B, et al. 2009. Acromial insufficiency in reverse shoulder arthroplasties. J Shoulder Elbow Surg 18:495-502.

43. Hamid N, Connor PM, Fleischli JF, et al. 2011. Acromial fracture after reverse shoulder arthroplasty. Am J Orthop (Belle Mead NJ) 40:E125-129.

44. Boileau P, Chuinard C, Roussanne Y, et al. 2007. Modified latissimus dorsi and teres major transfer through a single delto-pectoral approach for external rotation deficit of the shoulder: as an isolated procedure or with a reverse arthroplasty. J Shoulder Elbow Surg 16:671-682.

45. Jost B, Gerber C. 2004. Pectoralis Major Transfer for Subscapularis Insufficiency. Techniques in Shoulder & Elbow Surgery 5:157-164.

46. Giles JW, Boons HW, Ferreira LM, et al. 2011. The effect of the conjoined tendon of the short head of the biceps and coracobrachialis on shoulder stability and kinematics during in-vitro simulation. J Biomech 44:1192-1195.

47. Favre P, Senteler M, Hipp J, et al. 2012. An integrated model of active glenohumeral stability. J Biomech 45:2248-2255.

48. Adams CR, Baldwin MA, Laz PJ, et al. 2007. Effects of rotator cuff tears on muscle moment arms: a computational study. J Biomech 40:3373-3380.

49. Delille R, Bennani B, Lesueur D, et al. 2013. Experimental protocol to characterise damage of appendicular bone. Comput Methods Biomech Biomed Engin 16 Suppl 1:284-286.

FIGURE CAPTIONS

Figure 1: Diagrams illustrating rigid-body musculoskeletal model with the scapular reference frame shown (A) and finite element model of shoulder after reverse total shoulder arthroplasty, including scapula, humerus, glenosphere, humeral liner, base plate, and superior and inferior baseplate fixation screws (B). The scapular reference frame, in which glenohumeral joint force was expressed, was positioned at the centre of a sphere fitted to the glenosphere, with the x axis defined by a vector parallel to the line passing from the triangular surface of the medial border of the scapula to the centre of the acromioclavicular joint; the z axis was defined by a line passing vertically upward from the centre of the glenosphere and parallel to the plane of the base-plate surface; and the y axis was perpendicular to the x and z axes.

Figure 2: Finite element model simulations illustrating von Mises stress distributions at the glenosphere, baseplate, superior and inferior baseplate fixation screws and scapula at 45° of scapular plane abduction. Data are provided for the case of an intact rotator cuff; isolated supraspinatus (Supra) tear; combined supraspinatus and infraspinatus (Infra) tear; and

combined supraspinatus, infraspinatus and subscapularis (Subs) tear. Glenospheres are oriented with superior direction oriented upward and the anterior direction to the right. Red crosses indicate peak contact pressure locations.

Figure 3: Finite element model simulations illustrating von Mises stress distributions at the glenosphere, baseplate, superior and inferior baseplate fixation screws and scapula at 45° of sagittal plane flexion. See Figure 2 caption.

		Intact rotator cuff			Supra tear			Supra and Infra tear			Supra, Infra, and Subs tear			Supra, Infra, Tmin, and Subs tear		
		15◦	45◦	90◦	15◦	45◦	90◦	15◦	45◦	90◦	15◦	45◦	90◦	15◦	45◦	90◦
Abduction	Anterior deltoid	29.4	52.2	126.8	68.2	116.7	126.9	116.1	180.6	251.1	116.0	180.6	251.1	116.0	180.6	251.1
	Middle deltoid	74.8	206.8	240.7	116.6	225.5	240.5	135.1	177.2	155.2	135.1	177.2	155.2	135.1	177.2	155.2
	Posterior deltoid	0.0	0.0	24.6	0.0	0.0	23.9	0.0	0.0	0.0	0.0	0.0	0.0	0.0	0.0	0.0
	Supraspinatus	83.4	128.7	2.1	0.0	0.0	0.0	0.0	0.0	0.0	0.0	0.0	0.0	0.0	0.0	0.0
	Infraspinatus	76.2	168.5	214.2	159.2	256.2	214.4	0.0	0.0	0.0	0.0	0.0	0.0	0.0	0.0	0.0
	Subscapularis	80.3	220.4	207.8	162.8	302.8	207.3	0.0	0.0	0.0	0.0	0.0	0.0	0.0	0.0	0.0
	Teres minor	0.0	0.0	0.0	0.0	0.0	0.0	0.7	10.9	36.3	0.7	10.9	36.3	0.7	10.9	36.3
	Teres major	0.0	7.0	24.2	0.0	4.6	24.1	0.0	0.0	0.0	0.0	0.0	0.0	0.0	0.0	0.0
	Superior pectoralis major	0.0	0.0	186.7	0.0	0.0	187.0	41.3	45.9	51.7	41.4	45.9	51.7	41.4	45.9	51.7
Flexion	Anterior deltoid	56.0	105.3	155.3	83.1	128.7	154.5	97.1	199.8	298.9	91.6	199.8	298.9	91.6	199.8	298.9
	Middle deltoid	26.3	85.0	182.4	78.1	203.7	183.6	114.3	146.5	139.7	125.1	146.5	139.7	125.1	146.5	139.7
	Posterior deltoid	0.0	0.0	0.0	0.0	0.0	0.0	0.0	0.0	0.0	0.0	0.0	0.0	0.0	0.0	0.0
	Supraspinatus	73.5	133.2	2.2	0.0	0.0	0.0	0.0	0.0	0.0	0.0	0.0	0.0	0.0	0.0	0.0
	Infraspinatus	60.0	153.2	242.6	130.4	252.0	242.9	0.0	0.0	0.0	0.0	0.0	0.0	0.0	0.0	0.0
	Subscapularis	61.1	125.5	57.8	155.6	295.7	57.8	8.3	0.0	0.0	0.0	0.0	0.0	0.0	0.0	0.0
	Teres minor	0.0	0.0	7.1	0.0	0.0	7.1	0.0	10.8	97.7	0.0	10.8	97.7	0.0	0.0	0.0
	Teres major	0.0	0.0	0.0	0.0	3.9	0.0	0.0	0.0	0.0	0.1	0.0	0.0	0.1	0.0	0.0
	Superior pectoralis major	0.1	66.4	109.8	0.0	50.4	110.1	45.7	18.9	0.0	66.5	18.9	0.0	66.5	18.9	0.0

	Intra-operative screw loading	Intact rotator cuff	Supra tear	Supra and Infra tear	Supra, Infra, and Subs tear	Supra, Infra, Tmin, and Subs tear

	15◦	45◦	90◦	15◦	45◦	90◦	15◦	45◦	90◦	15◦	45◦	90◦	15◦	45◦	90◦	15◦	45◦	90◦
Superior Screw, Peak Stress (MPa)	5.8	10.8	10.7	66.3	100.5	159.3	81.1	104.7	159.0	32.2	31.7	113.1	32.1	31.7	113.1	31.4	24.7	119.3
Inferior Screw, Peak Stress (MPa)	7.9	8.1	8.1	7.9	13.6	12.1	9.7	15.1	12.1	12.2	9.3	7.5	12.2	9.3	7.5	12.0	8.5	7.9
Glenosphere, Peak Stress (MPa)	0.0	0.0	0.0	16.1	30.2	27.5	20.0	34.2	27.4	13.4	13.4	13.4	13.4	13.4	13.4	13.4	13.4	13.4
Glenosphere, Contact Force Rx (N)	0.0	0.0	0.0	-270.7	-608.9	-574.5	-367.1	-675.5	-572.9	-64.9	-76.9	-105.5	-64.8	-76.9	-105.5	-62.8	-50.3	-23.5
Glenosphere, Contact Force Ry (N)	0.0	0.0	0.0	-4.0	-6.6	-27.5	-3.2	-3.3	-27.4	-2.4	-1.7	-3.0	-2.4	-1.7	-3.0	-2.2	-1.6	0.0
Glenosphere, Contact Force Rz (N)	0.0	0.0	0.0	-44.9	-66.0	60.7	-63.0	-87.4	60.4	11.4	13.3	18.5	11.4	13.2	18.5	11.0	8.8	4.1
Glenosphere, Contact Force Magnitude (N)	0.0	0.0	0.0	274.4	612.5	578.3	372.5	681.2	576.7	65.9	78.0	107.2	65.8	78.1	107.2	63.8	51.1	23.9
Base Plate, Peak Stress (MPa)	13.4	13.4	13.4	13.5	20.1	21.1	13.8	23.6	21.1	13.4	13.4	13.4	13.4	13.4	13.4	13.4	13.4	13.4
Humeral Spacer, Peak Contact Pressure (MPa)	0.0	0.0	0.0	8.5	8.4	9.4	9.3	9.1	9.4	3.1	2.6	2.6	3.1	2.6	2.6	3.0	1.5	1.0
Humeral Spacer, Peak Stress (MPa)	0.0	0.0	0.0	8.5	9.2	8.1	9.3	10.4	8.0	3.1	3.0	3.2	3.1	3.0	3.2	3.0	1.7	1.1
Humerus Stem, Peak Stress (MPa)	0.0	0.0	0.0	7.5	10.9	13.4	9.3	12.3	13.3	2.8	2.6	4.2	2.8	2.6	4.2	3.0	2.7	1.6
Scapula, Peak Stress (MPa)	24.7	24.7	24.7	25.1	48.9	59.4	29.9	57.8	59.5	24.8	24.8	24.8	24.8	24.8	24.8	24.8	24.8	24.8

	Intra-operative screw loading			Intact rotator cuff			Supra tear			Supra and Infra tear			Supra, Infra, and Subs tear			Supra, Infra, Tmin, and Subs tear		
	15◦	45◦	90◦	15◦	45◦	90◦	15◦	45◦	90◦	15◦	45◦	90◦	15◦	45◦	90◦	15◦	45◦	90◦
Superior Screw, Peak Stress (MPa)	11.0	10.9	9.8	71.6	128.8	125.0	92.8	147.7	124.6	43.4	50.6	66.0	43.9	50.6	64.0	43.9	50.6	58.5

Inferior Screw, Peak Stress (MPa)	8.1	8.1	8.2	17.2	25.1	12.0	20.3	27.1	12.0	17.9	20.9	11.4	17.9	20.9	15.4	17.9	20.9	15.4
Glenosphere, Peak Stress (MPa)	0.0	0.0	0.0	13.5	17.4	33.1	13.5	23.2	33.0	13.4	13.4	13.6	13.4	13.4	13.4	13.4	13.4	13.4
Glenosphere, Contact Force Rx (N)	0.0	0.0	0.0	-181.2	-414.4	-322.6	-265.6	-513.4	-321.2	-63.4	-58.6	-110.6	-64.7	-58.6	-92.6	-64.7	-58.6	-77.2
Glenosphere, Contact Force Ry (N)	0.0	0.0	0.0	-48.2	-250.6	-357.1	-71.5	-307.3	-355.8	-29.1	-60.7	-134.4	-29.8	-60.7	-112.8	-29.8	-60.7	-96.2
Glenosphere, Contact Force Rz (N)	0.0	0.0	0.0	-30.3	-77.7	-14.6	-45.5	-97.6	-14.8	10.5	14.3	15.5	10.2	14.3	24.2	10.2	14.3	21.4
Glenosphere, Contact Force Magnitude (N)	0.0	0.0	0.0	189.9	490.5	481.5	278.8	606.2	479.6	70.5	85.6	174.8	71.9	85.6	148.0	71.9	85.6	125.2
Base Plate, Peak Stress (MPa)	13.4	13.4	13.4	13.5	17.4	18.1	13.5	21.8	18.1	13.4	13.4	13.4	13.4	13.4	13.4	13.4	13.4	13.4
Humeral Spacer, Peak Contact Pressure (MPa)	0.0	0.0	0.0	6.2	8.3	8.7	6.8	8.9	8.7	2.7	3.7	3.4	2.8	3.7	3.8	2.8	3.7	3.1
Humeral Spacer, Peak Stress (MPa)	0.0	0.0	0.0	6.4	8.5	9.5	7.0	10.2	9.4	2.9	4.1	3.9	3.0	4.1	4.2	3.0	4.1	3.5
Humerus Stem, Peak Stress (MPa)	0.0	0.0	0.0	6.1	13.8	19.8	8.8	21.6	19.8	6.8	6.8	19.1	7.0	6.8	17.4	7.0	6.8	15.9
Scapula, Peak Stress (MPa)	24.7	24.7	24.7	24.9	25.0	24.6	25.0	31.1	24.6	24.7	24.6	24.6	24.7	24.6	24.6	24.7	24.6	24.6

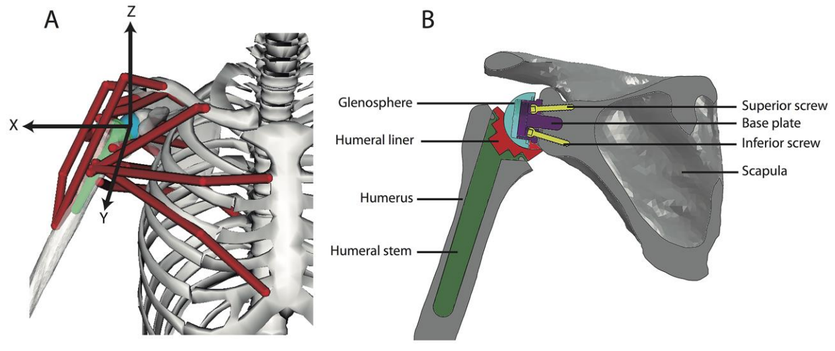

Figure 1 .

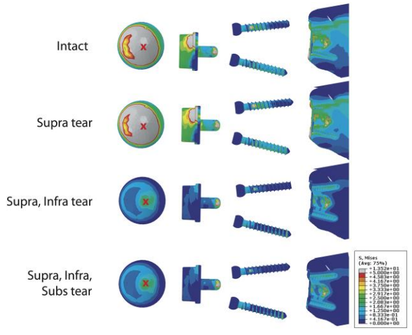

Figure 2 .

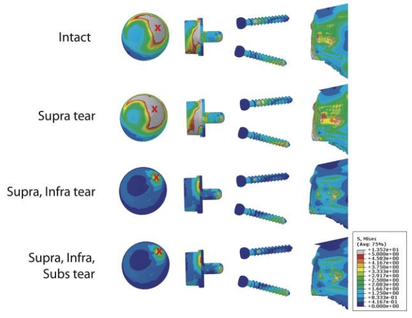

Figure 3 .